SSRG International Journal of Civil Engineering
ISSN: 2348-8352/ https://doi.org/10.14445/23488352/IJCE-V13I9P116

Volume 13 Issue 9, 273-283, September 2026

Original Article

Effect of Rainfall Infiltration on the Hydromechanical Behavior of Slopes under Unsaturated Conditions

Daira Ariadna Gonzalez Inca[1], Juan Gabriel Benito Zuñiga[2]

[1]School of Civil Engineering, Universidad Continental, Huancayo, Peru.
[2]Department of Geotechnical Engineering, Polytechnic University of Valencia, Valencia, Spain.

[1]Corresponding Author : 77351475@continental.edu.pe

Received: 03 June 2026 Revised: 02 September 2026 Accepted: 07 September 2026 Published: 29 September 2026

Abstract *- Nowadays, slopes forming transportation infrastructure are highly sensitive to hydraulic conditions such as rainfall, triggering negative impacts on ecosystems and road infrastructure. In this regard, this research analyzes the hydromechanical influence of a frequent rainfall intensity in northern Peru of 10 mm/h on the stability of slopes (T1, T2, and T3) under unsaturated conditions. For this purpose, simulations were performed using Plaxis 2D software, considering three slope geometries based on regulatory criteria for clayey gravel soils with fines content and groundwater table conditions. The input parameters for the soil were based on the Hardening Soil model, while the Van Genuchten model was used for flow analysis. The obtained results indicate that, within the analyzed section measured from the upper surface downward, maximum saturation reached a depth equivalent to 33% of the slope height for model T1, 11.8% for model T2, and 6.4% for model T3. In addition, the effective surface suction produced reductions lower than 3 kN/m² after 24 hours of continuous rainfall. Finally, the factor of safety was affected under the same scenario, decreasing by up to 59.11% for model T1, 49.2% for model T2, and 42.80% for model T3. It should be noted that the most significant transition toward instability occurred after 10 hours.*

Keywords *- Rainfall infiltration, Slope, Hydromechanical behavior, Suction, Saturation.*

1. Introduction

One of the main pillars of transportation infrastructure is the geotechnical sector, within which slopes are considered and vary according to the topography of each national territory. However, over time, these structures have shown sensitivity to hydraulic conditions, particularly under rainfall effects, bringing adverse consequences to urban planning, infrastructure safety, and ecosystem loss [1, 2]. Another issue is the inherent susceptibility of soils, as in the case of Peru, where susceptibility maps for mass movement have been developed by the Geological, Mining, and Metallurgical Institute (INGEMMET) for different rainfall thresholds according to hydrological studies carried out by SENAMHI [3, 4]. Rainfall infiltration causes slope stability problems because it changes the hydraulic properties inside the slope, mainly triggering landslides. However, few studies address the infiltration limits that affect slope stability [5].

Soil infiltration occurs when water moves vertically into the ground. This increases the soil moisture content, changes pore water pressure and strength parameters, and affects soil stability [6-8]. When slope failures occur due to rainfall-induced landslides, their importance lies in the economic paralysis caused by the lack of access between connected regions. Likewise, carrying out large-scale earthworks requires substantial economic investment [9]. Therefore, studying these phenomena is essential to develop preventive procedures.

Throughout time, multiple investigations related to this topic have been conducted [10, 11]. However, less realistic cases have often been considered, such as soil without groundwater tables and strong rainfall intensities of up to 30 mm/h for prolonged durations of 24 hours [12]. According to reports from the National Service of Meteorology and Hydrology of Peru (SENAMHI), moderate estimated precipitation events of up to 10 mm/h occur in the southwestern regions covering different jungle sectors [13, 14].

As mentioned above, rainfall infiltration causes changes within the soil. For this reason, it is important to define its stiffness and strength properties to represent the resulting deformations realistically. In this context, the Hardening Soil constitutive model represents a nonlinear elastoplastic behavior that incorporates hardening under both compression and shear conditions. The importance of this method lies in the dependence of stiffness on stress conditions, plastic deformations, and the yield surface [15]. In addition, it determines stiffness through small-strain behavior and its degradation under cyclic loading conditions.

Other important aspects within the soil are matric suction and moisture content, which can be assessed through the degree of saturation to help prevent slope failures. The suction curve can also be used to measure the water retention capacity and hydraulic behavior of unsaturated soil. To evaluate this phenomenon, the Van Genuchten model is generally used, which is implemented in Plaxis 2D software with realistic parameters for a better representation of the model under rainfall infiltration effects on slope stability [15].

Likewise, studies have been carried out regarding the infiltration effect on two types of soils: well-graded sand (SW-SM) with high fines content, which experienced a considerable reduction in the factor of safety [12]; however, another soil type, poorly graded sand (SP-SM) with lower fines percentages under unsaturated conditions, exhibited lower sensitivity to infiltration while maintaining a relatively constant factor of safety [12]. Nevertheless, these case studies do not consider groundwater levels, and SW-SM soils exhibit greater long-term sensitivity due to the reduction in the factor of safety, reaching instability conditions after 24 hours of infiltration. On the other hand, the selected study material corresponds to a transitional soil between SP-SW and SW-SM soils, containing a lower proportion of fines and higher permeability compared to SP-SW soils.

There are studies on rainfall infiltration considering different slope geometries [16], but only a few cases additionally include infiltration effects using rainfall intensity and duration [17]. However, more practical geometries are not proposed, such as Vertical-to-Horizontal (V:H) ratio configurations recommended by the Peruvian Highway Design Manual (DG-2018) for slopes [18]. Table 1 presents key studies by different authors. However, these studies have some limitations, leaving several technical questions unanswered.

Table 1. Key studies in the literature

Study	Finding	Limitation
[5]	The study indicates that soil density may increase during the early stages of infiltration on the slope face. However, the gradual increase in moisture reduces the friction coefficient and cohesion.	It uses only one slope configuration (1H:2V) and a rainfall intensity of 18 mm/day.
[6]	This study found that rainfall infiltration at an intensity of 20 mm/h is a key factor in the stability of slopes made of high-plasticity silt.	Although it analyzes rainfall infiltration at 10 mm/h, the soil used is high-plasticity silt, and the permeability at which this behavior occurs is not quantified.
[16]	This study found that, in slopes with a defined groundwater table and suction above it, suction tends to decrease and the water level rises due to downward flow from rainfall.	The soils used were sandy clay and clay, with permeabilities of 1E-6 and 1E-8, respectively. Infiltration was considered for only up to 12 hours.
[12]	This study found that well-graded sand (SW-SM) showed a considerable reduction in its factor of safety as rainfall duration gradually increased.	It considered only one slope geometry, with a rainfall intensity of 30 mm/h and a duration of 24 hours. These conditions are not very realistic for areas with frequent rainfall.
[17]	This study found that low-intensity rainfall over a long period significantly affects slope stability, particularly on the slope face. It also found that the factor of safety decreases more in gentler slopes than in steeper ones.	The study focuses on high-plasticity silt. Although it considers several rainfall intensities, it does not analyze an intensity of 10 mm/h or progressively longer durations for each intensity.

Table 1 shows that some studies analyze one or several slope geometries, but these are not based on design standards or technical guidelines. A more realistic rainfall intensity of 10 mm/h is also generally not used. When this intensity is considered, the duration is not prolonged. In addition, these studies rarely examine clayey gravel soils, which are more permeable than fine soils.

Experimental monitoring of water pressure and moisture content helps predict the development of landslides. However, too few monitoring points make it difficult to obtain a complete picture of saturation, water suction, and effective stresses within the slope [19]. Therefore, numerical simulations are needed as a complementary tool to evaluate the effects of rainfall infiltration on slopes [5].

Using Peru as a reference, this study analyzes infiltration under a common rainfall intensity of 10 mm/h and includes the groundwater table as a realistic parameter for specific conditions in soils that are more permeable than fine soils. The study also uses slope geometries based on design standards and evaluates key aspects of hydromechanical behavior, including matric suction, degree of saturation, and stability through the factor of safety.

2. Materials and Methods

2.1. Soil Characterization and Constitutive Model

The selection of the soil classification was obtained from the research conducted by [13], where Table 2 presents the geotechnical characteristics.

Table 2. Soil properties

Characteristics	Symbol	Value
Saturated unit weight (kN/m^3)	γ_{sat}	20
Unsaturated unit weight (kN/m^3)	γ_{unsat}	19
Gravel (%)	G	48.4
Sand (%)	S	13.1
Silts and clays (%)	F	38.5

The cohesion and friction angle values present coherent adjustments for Clayey Gravel Soil (GC), since the friction angle range varies between 30°–40° for well-graded and poorly graded sands, while cohesion ranges between 0 and 20 kN/m^2. However, cohesion largely depends on the compaction level and the amount of fines present. The proposed selection of this soil is associated with the extensive use of quarry extraction materials employed as fill material for roads [20] or for the construction of embankments in mining sites [13].

The Hardening Soil constitutive model was used to represent the mechanical behavior of the soil. It is based on a nonlinear elastoplastic approach that includes shear and compressive strength. Although this model requires more input data, it provides promising results for geotechnical applications because it represents actual conditions more closely [20]. First, a Consolidated-Drained (CD) triaxial compression test was carried out using effective confining pressures (σ_3) of 200 kPa, 400 kPa, and 800 kPa. After obtaining the deviator stress ($\Delta\sigma$) for each strain (ε), 50% of the maximum deviator stress was calculated. This value was then divided by its corresponding interpolated strain (ε_1) to obtain the secant modulus of elasticity for each confining pressure (Table 3).

Table 3. Calculation of E_{50} for each confining pressure

	σ_3 800 (kPa)	σ_3 400 (kPa)	σ_3 200 (kPa)
50% $\Delta\sigma_{max}$ (kPa)	667	366.5	199.5
ε_1	0.0231	0.024	0.0287
E_{50} (kN/m^2)	28914.3	15251.4	6953.5

By correlating the E_{50} moduli with the confining pressures described in Table 2, a value of 1.028 was obtained for "m" using a power-law regression. To calibrate the elastic moduli (E_{50}, E_{oed}, E_{ur}) and strength parameters (c`, ϕ`), a confining pressure of 100 kPa or higher is generally used to obtain the reference secant modulus ($E_{50\ ref}$). In this case, the intermediate confining pressure of the three values (400 kPa) was used with its corresponding secant modulus ($E_{50\ ref}$ =15 251.4 kN/m^2). Some empirical correlations [21] estimate the other variables (E_{oed}, E_{ur}) by using 85% of $E_{50\ ref}$ to estimate E_{oed} and 4 times $E_{50\ ref}$ to estimate E_{ur}.

Table 4 shows the strength and stiffness parameters of this constitutive model. These were calibrated using the triaxial tests described in the previous paragraphs.

Table 4. Hardening soil model parameters

Characteristics	Symbol	Value
Dilatancy angle	ψ	0
Secant stiffness modulus (kN/m^2)	E_{50}	15 251.4
Oedometer stiffness modulus (kN/m^2)	E_{oed}	12 963.7
Unloading/reloading stiffness modulus (kN/m^2)	E_{ur}	61 005.5
Effective cohesion (kN/m^2)	c`	10
Effective friction angle (º)	ϕ`	30.5
Poisson's ratio	V_{ur}	0.29
Power exponent	m	1

2.2. Hydraulic Parameters

This study uses the Soil-Water Retention Curve (SWCC), based on the Van Genuchten model described in Equation 1, which relates soil moisture content to suction.

$$\theta = \theta_r + \frac{(\theta_s - \theta_r)}{[1 + (\alpha h)^n]^m} \quad (1)$$

$$m = 1 - \frac{1}{n} \quad (2)$$

Where the four main independent parameters (θr, θs, α, and n) must be estimated from the soil-water retention curve. First, the saturated water content (θr) can be easily obtained from experimental data and estimated through observation of soil water content. Another parameter, residual water content (θs), is obtained from the water content in very dry soil conditions. The variable "m" can be estimated from the slope (dθ/dh) and pressure head (h) at a certain point along the θ(h) curve [22].

Effective saturation "S_{eff}" is determined using Equation 3. Effective pressure "ρ_{eff}" is then obtained from Equation 4, followed by the effective soil stress "σ'" using Equation 5.

$$S_{eff} = \frac{Sr(\Psi) - S_{res}}{S_{sat} - S_{res}} \quad (3)$$

$$\rho_{eff} = S_{eff} * \rho_w \quad (4)$$

$$\sigma' = \sigma - \rho_{eff} \quad (5)$$

Here, "S_{eff}" is the effective degree of saturation, "$S_r(\Psi)$" is the saturation level as a function of suction, "S_{sat}" is the total soil saturation, "p_w" is the water pressure, "S_{res}" is the residual saturation, and "σ" is the total stress. Plaxis 2D uses different variables that are proportionally equivalent to those in Equations 1 and 2: S_{res}, S_{sat}, g_a, g_c, g_n) [12].

To evaluate flow behavior, Plaxis 2D also describes changes in pressure through suction [12], using Equation 6.

$$\frac{dS(p_w)}{dp_w} = (S_{sat} - S_{res})\left[\frac{1-g_n}{g_n}\right]\left[g_n\left(\frac{g_a}{\gamma_w}\right)^{g_n} . p_w{}^{(g_n-1)}\right]\left[1 + \left(g_a . \frac{p_w}{\gamma_w}\right)^{g_n}\right]^{\left(\frac{1-2g_n}{g_n}\right)} \quad (6)$$

Where "γ_w" is the unit weight of water. The suction curve shown in Figure 1 was obtained from the research conducted by [13]. Based on this adjustment, the parameters for the Van Genuchten model were derived, as shown in Table 5.

Table 5. Van Genuchten model parameters

Variables	GC Soil
Permeability (m/day)	8.64
$S_{res} = \theta_{res}$	0.05
$S_{sat} = \theta_{sat}$	1.00
$g_a = \alpha$ (m^{-1})	1.79
$g_n = n$	1.20
$g_l = -m$	0.50

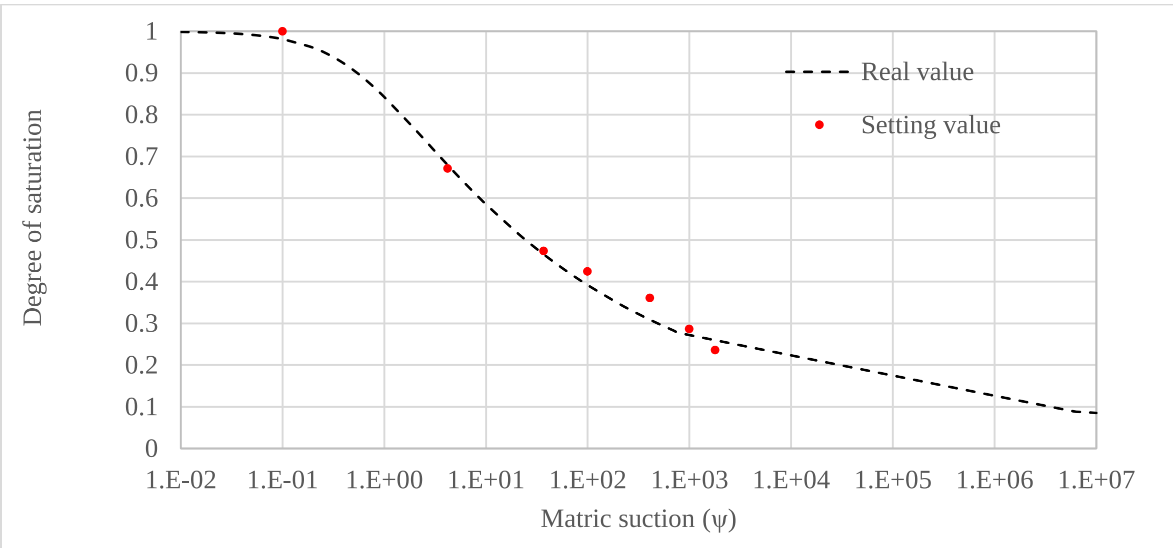

Fig. 1 Suction curve model for GC soil

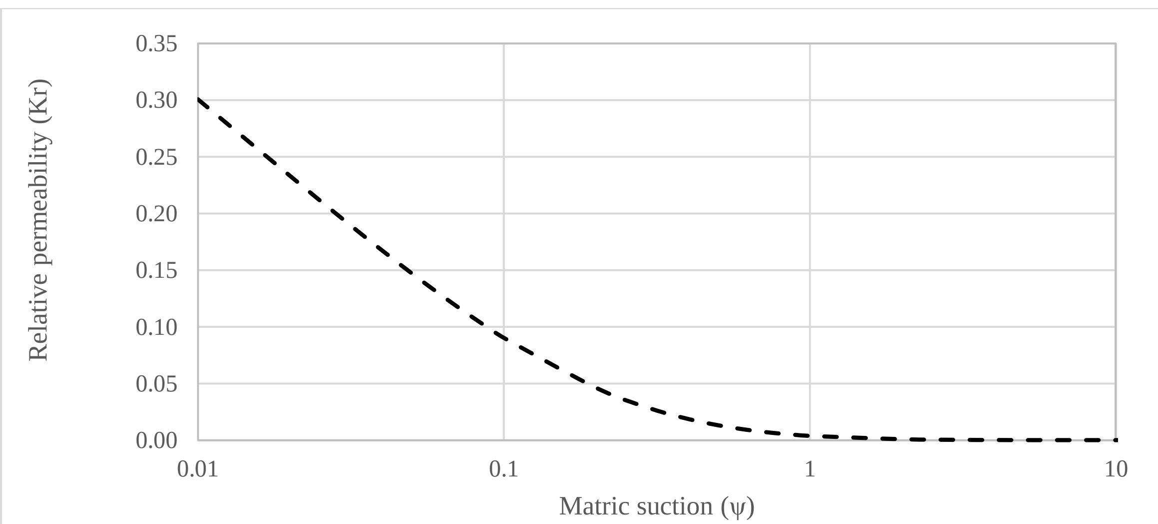

Fig. 2 Variation of permeability as a function of soil suction

The permeability used in Table 4 falls between that of soils with a low fines content (1x10^{-3} m/s) and a high fines content (1x10^{-5} m/s). These soils are described as having low permeability due to changes caused by weathering, cracking, and drying [23].

On the other hand, in moderately saturated soils, permeability varies according to water content, known as relative permeability (k_r), since the amount of water within the pores is altered due to suction.

This changes the soil's ability to permit water flow. This process is evaluated using the expression shown in Equation 5, thus obtaining the relative permeability model as a function of suction presented in Figure 2.

$$K_r = \max\left({S_{eff}}^{g_l} \left[1 - \left({S_{eff}}^{\frac{-1}{g_c}} \right)^{-g_c} \right]^2 ; \ 10^{-4} \right) \tag{7}$$

2.3. Slope Geometry and Boundary Conditions

The selection of slope geometry (V:H) was based on configurations described in the Highway Geometric Design Manual [19], where slopes are classified according to slope height and soil material, as shown in Table 6.

Table 6. Reference slopes in fill areas

Material	Slope (V:H)		
	Height (m)		
	< 5	5 – 10	> 10
Gravel, sandy silt, and clay	1:1.5	1:1.75	1:2
Sand	1:2	1:2.25	1:2.5
Rockfill	1:1	1:2.25	1:1.5

Based on the selected soil type, the material corresponding to gravels, sandy silts, and clays was considered for the three slope heights. Furthermore, these configurations correspond to slopes with greater susceptibility compared to other geometries [18] and possess normative relevance.

Therefore, the geometric configurations of the studied slopes are presented in Table 7 and represented in Figure 3. These configurations allow the analysis of highly inclined slopes with considerable height.

Table 7. V:H ratio in slope geometry

Slope	Vertical	Horizontal	Groundwater Level
	V (m)	H (m)	G.L. (m)
T1	4	6	- 5.0
T2	8	14	
T3	12	24	

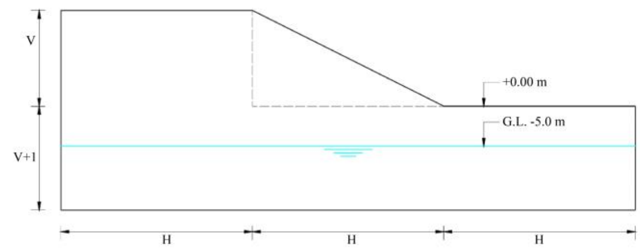

Fig. 3 Geometric configuration of the slope

The slope analysis is carried out in the section indicated in Figure 4. It should be noted that the selected section provides better visualization of the variations within the soil layer and their effects along the slope component, allowing a more accurate evaluation of stability and soil behavior.

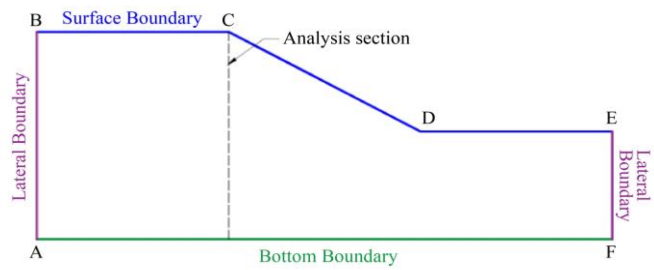

Fig. 4 Analysis section and components of the boundary condition

On the other hand, to establish the boundary conditions of the numerical model, conditions were defined both for the soil material and for the flow conditions. Regarding the material conditions, a fixed condition was imposed at the base, meaning a restriction in both directions so that deformation cannot occur in either the ($u_x = u_y = 0$) directions. Along the lateral boundaries, deformation was restricted in the X direction while allowing deformation in the Y ($u_x = 0$) direction. At the ground surface, free deformation was allowed in both directions. These conditions are presented in Table 8.

Table 8. Boundary conditions for the material

Boundary	Material (Soil)
AB, EF (lateral)	$u_x = 0$
F,A (base)	$u_x = u_y = 0$
BC,CD,DE (surface)	-

Similarly, boundary conditions for water flow were established by imposing infiltration at the surface of the geometry. At the lateral boundaries, flow is allowed under a seepage condition and at the base, it is restricted by an impermeable condition. These conditions are presented in Table 9.

Table 9. Boundary conditions for flow

Boundary	Flow
AB, EF (lateral)	Seepage
FA (base)	Closed
BC,CD,DE (surface)	Infiltration

2.4. Rainfall Intensity Characterization

The selection of the rainfall intensity of 10 mm/h corresponds to common rainfall events occurring in northern Peru (Amazon rainforest region) during rainy seasons, although it may also occur in some areas of central Peru. The duration of this intensity rarely exceeds long periods (greater than 2 hours) [11]. However, in order to obtain critical scenarios and evaluate the degree of sensitivity of slopes to landslides, longer duration intervals were considered. Therefore, this research proposes durations of 2, 10, 18, and 24 hours.

2.5. Analysis Procedure

Once the input parameters described in the previous sections were defined: Material classification, constitutive model, hydraulic model, model geometry, rainfall characterization, and rainfall duration times. The next phase involved numerical modeling using Plaxis 2D software. Figure 5 presents the flowchart of the sequence of activities.

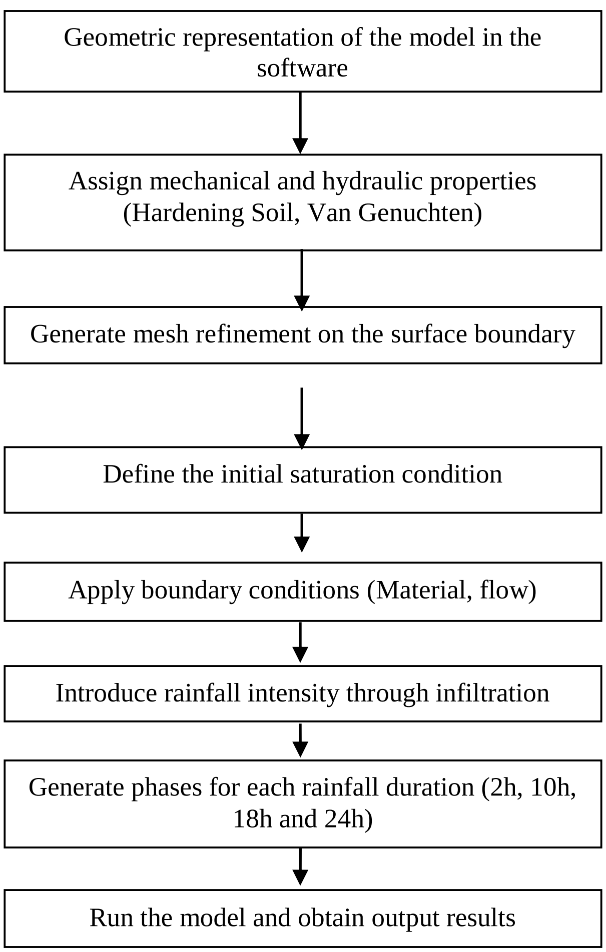

Fig. 5 Flowchart of Activities in Plaxis 2D Software

The numerical control parameters must be set before running the model in PLAXIS 2D. The values shown in Table 10 are used to ensure convergence and mathematical stability without introducing changes in the output results.

Table 10. Numerical control parameters

Description	Value
Maximum steps	100
Error tolerance	0.01
Maximum number of iterations	60
Desired minimum number of iterations	6
Desired maximum number of iterations	15

2.6. Study of Mesh Convergence

The slope geometry was meshed using 15-node triangular elements. Figure 6 shows the mesh for model T1 as an example.

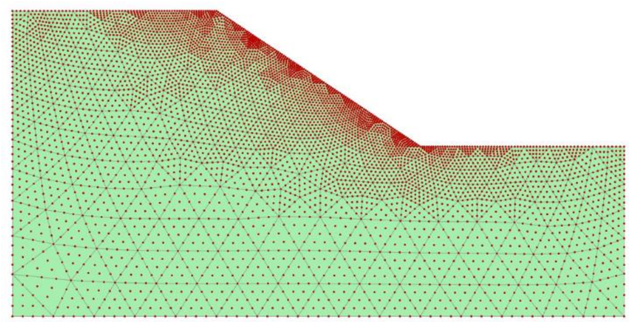

Fig. 6 Mesh of 15-node triangular elements in model T1

Good mesh stability can be achieved with element sizes starting at 500 mm. This size has been considered for different soils with friction angles of 8º and 30º and cohesion values of 38 and 15 kPa [24, 25]. However, to ensure better convergence, triangular element sizes from 2000 mm to 10 mm were evaluated. Figure 7 shows that the displacements converge, with negligible variation from 400 mm onward for model T1. The same behavior was also observed in models T2 and T3.

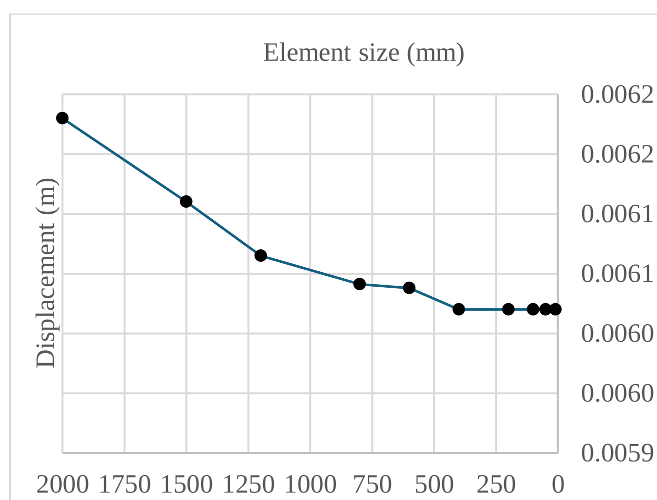

Fig. 7 Variation in output results for each mesh element size

3. Results

The initial hydraulic conditions (0 hours) were considered at the same level at G.L. = −5.0 m relative to the reference level (+0.00) for the three geometric slope configurations (T1, T2, and T3). Based on this water table condition, the initial distribution of suction and effective saturation was estimated by assuming hydrostatic equilibrium in the unsaturated zone. Under this assumption, suction will be greater the farther away from the water table, while effective saturation will decrease as depth decreases.

3.1. Degree of Saturation

Figure 8 shows the variation of the degree of saturation for model T1 under different rainfall durations. Initially, it can be observed that the saturation at the initial stage (0 hours), located at the slope surface, was 60%. After 2 hours, saturation progressively increased to 100% at the surface. Furthermore, saturation was not limited only to that zone; as rainfall duration increased (10, 18, and 24 hours), greater depths became saturated vertically along the slope. This phenomenon occurred similarly for models T2 and T3, although with initial saturation values of 56% and 53%, respectively.

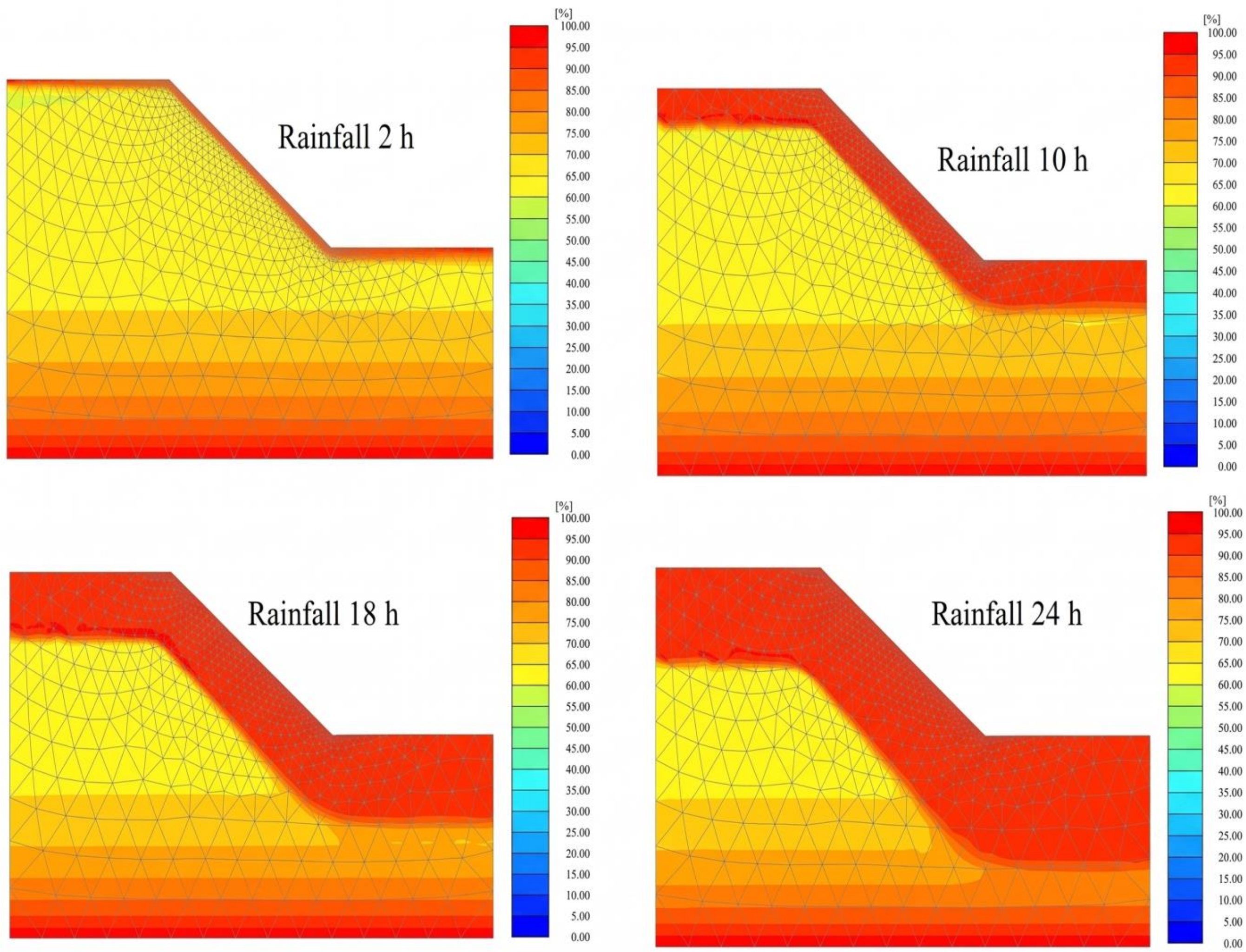

Fig. 8 Variation of saturation along the slope surface for each rainfall duration time

Figure 9 presents effective saturation profiles for the three slope cases, allowing the analysis of effective saturation in relation to rainfall duration and slope height. The three graphs exhibit a similar behavior: the surface zone (T1: 9 m, T2: 17 m, and T3: 25 m) interacts rapidly with infiltration. After 2 hours, effective saturation reaches values not lower than 90%. As rainfall progressively increases (10, 18, and 24 hours), saturation begins to propagate vertically downward through the soil, stabilizing around 94%, with the 24-hour duration producing the greatest infiltration depth within the slope. On the other hand, the effective saturation profile also shows a distribution that gradually decreases from the groundwater table condition toward the superficial layer of the slope. These three slope models show a relationship between slope height and effective saturation: as slope height increases, the depth reached by effective saturation decreases.

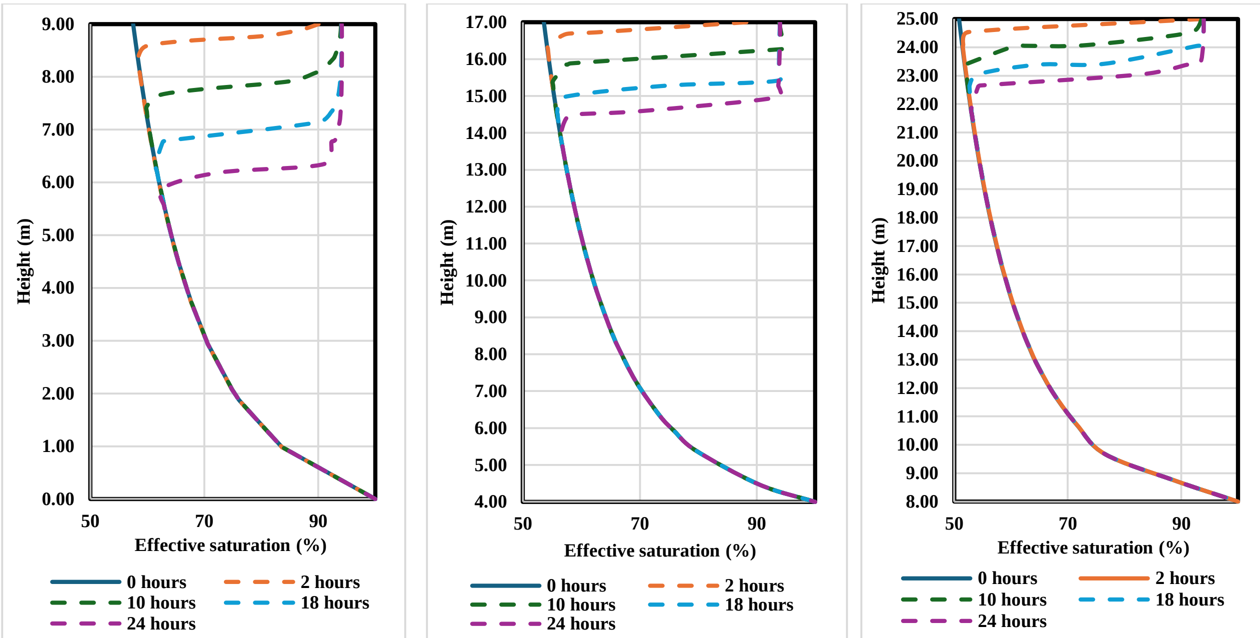

(a) (b) (c)

Fig. 9 Effective saturation in the analysis section for each duration time of each model (A: T1, B: T 2, C: T 3)

3.2. Suction

Figure 10 shows the variation of suction for model T1 under different rainfall duration times. Unlike saturation, this effect is inversely proportional; that is, when the degree of saturation increases, suction progressively decreases for all cases. Initially, the suction at the initial condition (0 hours), located at the slope surface, was 86 kN/m². After 2 hours, it progressively decreased to 76% at the surface. Likewise, suction alteration was not limited to this zone, since as rainfall duration increased (10, 18, and 24 hours), suction reductions extended to greater vertical depths within the analysis section. As expected, this phenomenon also occurred similarly for models T2 and T3, although with initial suction values of 124% and 163%, respectively.

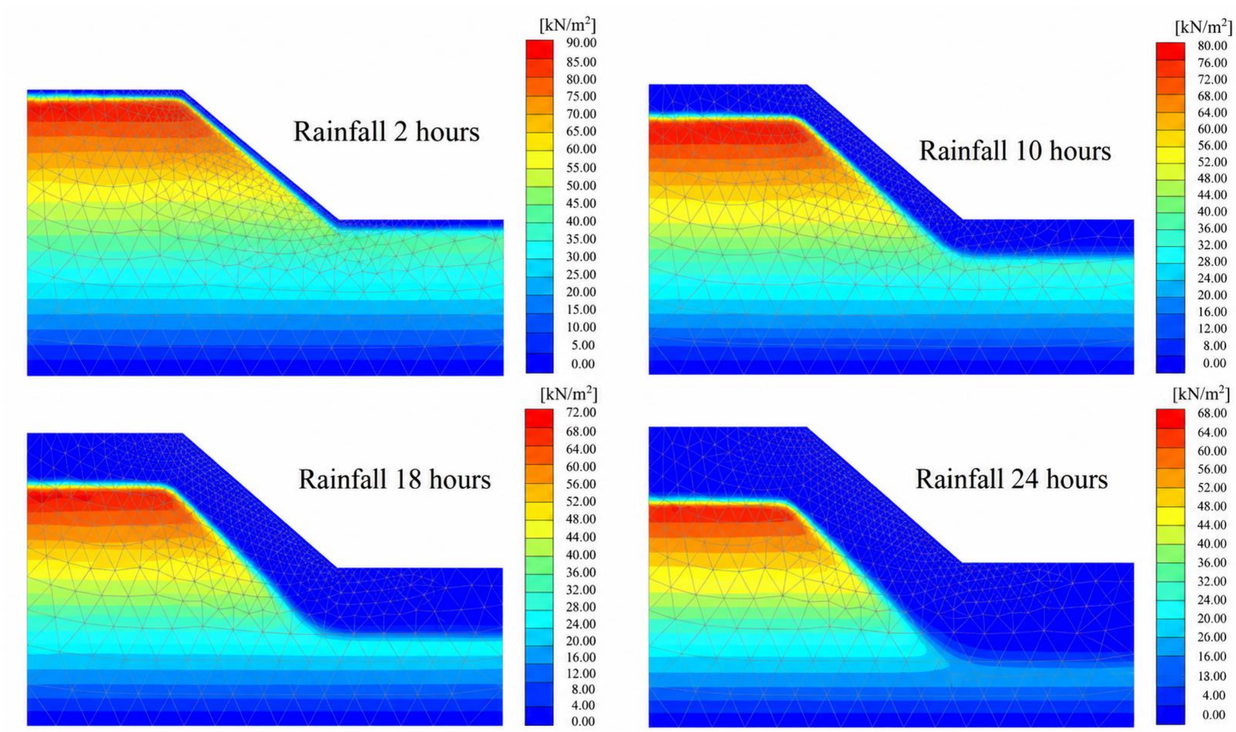

Fig. 10 Variation of suction along the slope surface for each rainfall duration time

Figure 11 presents the effective suction profiles for the three study scenarios, considering infiltration duration time and depth within each slope layer. In all three cases, the immediate response of effective suction to rainfall intensity can be observed. After 2 hours, a significant reduction occurs, reaching values lower than 9 kN/m². As rainfall duration increases (10 hours), suction further decreases to values lower than 3 kN/m², stabilizing during subsequent durations (18 and 24 hours). It should be noted that the initial effective suction gradually increases as the distance from the groundwater table toward the superficial soil layer becomes greater. The comparison of these slope geometries also shows that, as slope height increases, changes in effective suction reach a shallower depth.

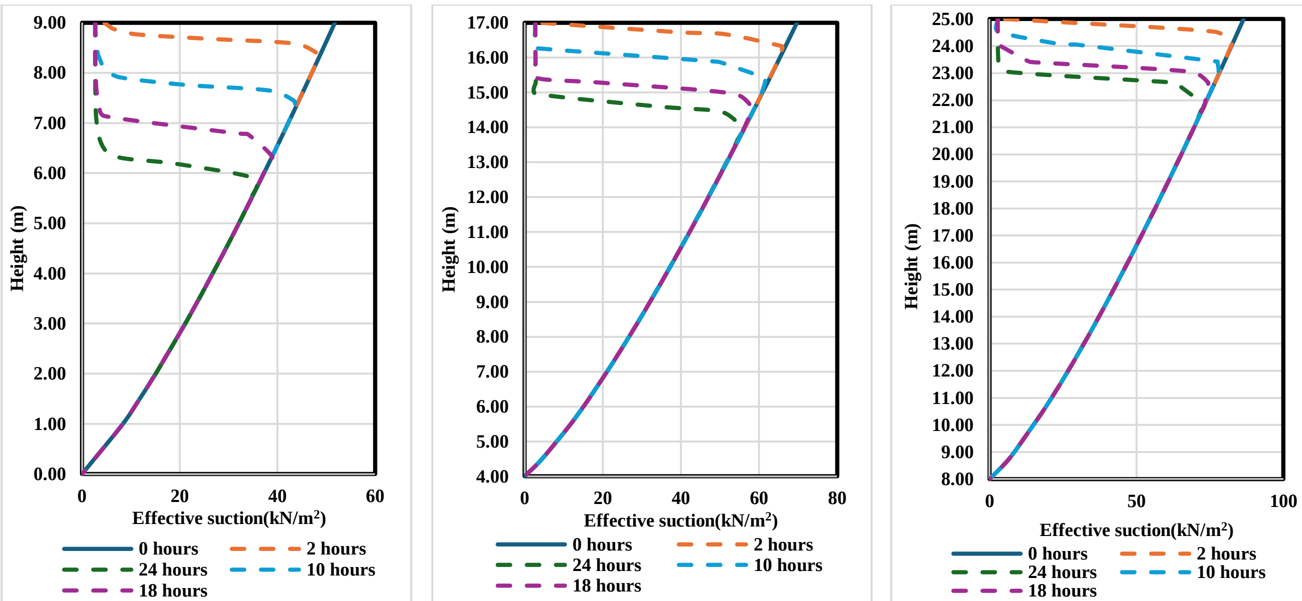

Fig. 11 Effective suction in the analysis section for each duration time of each model (A: T1, B: T 2; C: T 3)

3.3. Factor of Safety

Figure 12 presents the factor of safety as a function of rainfall infiltration duration for each slope geometric configuration. Initially, model T1 exhibited greater stability, with a factor of safety of 3.5 during the initial phase (0 hours), compared to models T2 and T3. As rainfall infiltration progressed for 2 hours, stability decreased proportionally in all three models. However, after 10 hours, the factor of safety dropped sharply, reaching an average value of approximately 1.75. As rainfall duration continued to increase, the factor of safety continued decreasing, although at a lower rate. Thus, after 24 hours of rainfall duration, the factor of safety reduction with respect to the initial condition reached up to 59.11% for model T1, 49.21% for model T2, and 42.80% for model T3. The geometry of each of these three slopes determines its factor of safety at the initial stage (0 h), while infiltration controls the later reduction in the factor of safety over time.

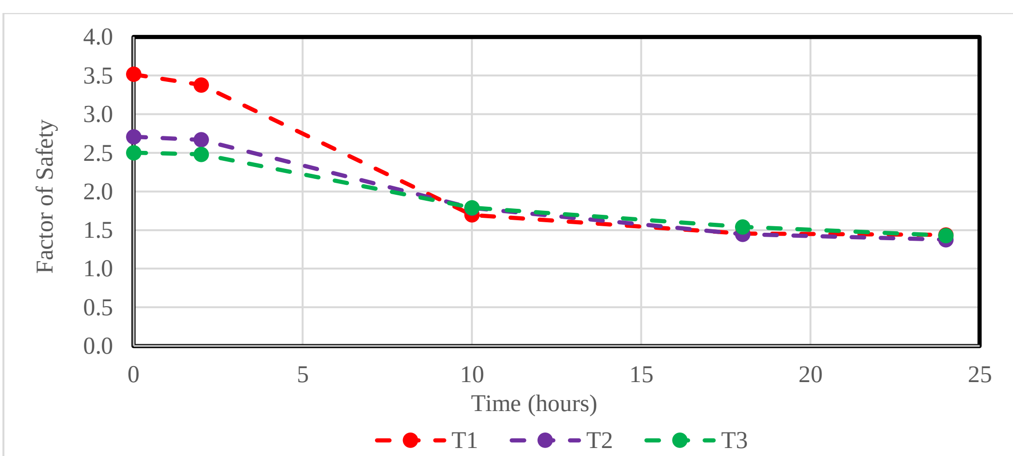

Fig. 12 Factor of safety versus rainfall duration time

4. Discussions

The saturation process in these clayey gravels exhibits a moderately slow behavior due to the concentration of fines within their composition [10, 25], reaching 100% saturation at a depth equivalent to approximately 33.3% of the analysis section measured from the slope surface in model T1 after 24 hours. As the analysis section increases, as in models T2 and T3, the saturation depth affects only 11.8% and 6.4%, respectively. Despite the presence of the groundwater table at the same position in all cases, maximum saturation does not occur at the base of the slope (V), remaining around 65%. This indicates that extreme propagation cases caused by rainfall infiltration are limited due to the low permeability of the soil [26]. On the other hand, the suction values obtained at the initial stage were high (approximately between 86 and 163 kN/m²) and progressively decreased as infiltration time increased, reaching depths equivalent to 0.56H, 0.22H, and 0.12H for models T1, T2, and T3, respectively (measured from the upper part of the slope). However, effective suction at the base of the slope (V) was not significantly affected, remaining around 31 kN/m². This indicates a greater suction retention capacity due to the silt content present in the material [27]. Furthermore, this demonstrates the clear relationship between soil gradation and its water retention capacity [12].

The factor of safety is another important parameter under rainfall infiltration effects, revealing that prolonged rainfall can significantly affect slope stability and increase landslide risk. This decreasing evolution of the factor of safety is associated with grain size distribution and the coefficient of uniformity due to pore dispersion and the hydraulic effect of soil stratigraphy [25], leading to greater moisture accumulation and gradually altering the factor of safety. Moreover, if the soil distribution is more uniform and the fines content is not excessively high, infiltration becomes faster but less deep, without significantly affecting suction in deeper zones, thereby producing a more stable material in the long term [12]. Likewise, under different slope configurations subjected to infiltration effects, model T1, despite presenting greater initial stability, does not necessarily guarantee better long-term performance compared to models (T2 and T3), since this behavior depends on soil composition and rainfall exposure duration. The factor of safety for model T2 decreased by 49.2% due to rainfall infiltration. This is similar to the case study in [28], which reported a reduction of 40% using PLAXIS 2D and compared the results with experimental tests on the slope face. The difference is mainly due to soil permeability, as the soil in our study is more permeable (k_s = $1x10^{-4}$ m/s). For infiltration analysis, PLAXIS 2D also gives conservative values compared with other commercial software such as SLIDE 2D, RS2, SEEP/W, and SLOPE/W. For slope stability analysis, it produces results similar to those obtained experimentally [28].

The main limitations of this study concern soil–vegetation interaction, surface roughness, and compaction. Although factors such as vegetation have been shown to reduce the impact on slope stability [29], their effects need to be quantified in future studies. The numerical results should therefore be used for simplified preliminary case studies and to assess unfavorable trends.

5. Conclusion

This study analyzed hydrodynamic behavior and its effect on slope stability in clayey gravel soils containing fines. Numerical simulations were carried out in Plaxis 2D under rainfall infiltration at an intensity of 10 mm/h to evaluate its effect on the three proposed slope geometries (T1, T2, and T3). The results showed that effective saturation and suction are influenced by slope geometry. As slope height increases, effective saturation and changes in effective suction reach shallower depths. Initial stability was also found to depend on slope geometry, while infiltration plays a key role in reducing the factor of safety over time. In particular, model T1 showed the largest reduction, at 59.11%, after 24 h of continuous rainfall infiltration. This behavior is attributed to its higher permeability compared with fine soils. In terms of flow, it also shows greater suction retention, while the gradual increase in saturation reduces soil strength. The initial factors of safety indicated stable conditions for all three slope geometries, with model T1 showing the highest stability. However, under rainfall-induced flow conditions, all models experienced a significant reduction in stability, becoming susceptible to instability under prolonged rainfall durations. Finally, some limitations of this study could be addressed in future research, including soil–vegetation interaction, surface roughness, and compaction. Field experiments are also needed to develop parametric models calibrated to realistic conditions.

References

[1] Tung-Lin Tsai, Hung-En Chen, and Jinn-Chuang Yang, "Numerical Modeling of Rainstorm-Induced Shallow Landslides in Saturated and Unsaturated Soils," *Environmental Geology*, vol. 55, no. 6, pp. 1269-1277, 2008. [CrossRef] [Google Scholar] [Publisher Link]

[2] Zechuang Li, and Zhiyi Yin, "Failure Pattern of Dispersive Soil Slopes under the Action of Rainfall Conditions," *Alexandria Engineering Journal*, vol. 104, pp. 193-210, 2024. [CrossRef] [Google Scholar] [Publisher Link]

[3] Waldo Lavado Casimiro et al., *SENAMHI Hydrological Study: Executive Summaries – 2020*, National Meteorology and Hydrology Service of Peru, pp. 1-113, 2020. [Google Scholar] [Publisher Link]

[4] Lionel Fidel Smoll et al., "*Map of Susceptibility to Mass Movements in Peru*," INGEMMET Institutional Repository, pp. 308-311, 2010. [Google Scholar] [Publisher Link]

[5] Jian Zhang et al., "Evaluation of the Effects of Rainfall Infiltration Boundaries on the Stability of Unsaturated Soil Slopes Using the Particle Flow Code," *Water*, vol. 16, no. 24, pp. 1-15, 2024. [CrossRef] [Google Scholar] [Publisher Link]

[6] Sohaib Naseer, and Robert Evans, "Effect of Rainfall Intensity and Duration on Stability of Natural Slopes of Unsaturated Fine Soils," *4th Conference on Sustainability in Civil Engineering (CSCE'22*, Islamabad Pakistan, pp. 1-7, 2022. [Google Scholar]

[7] AB Fourie, D. Rowe, and GE Blight, "The Effect of inÆltration on the Stability of the Slopes of a Dry Ash Dump," *Geotechnique Engineering*, vol. 49, no. 1, pp. 1-13, 1999. [CrossRef] [Google Scholar] [Publisher Link]

[8] D H Hsiao et al., "A Study on a Instability Slope in Taiwan Subjected to Rainfalls," *IOP Conference Series: Earth and Environmental Science: 2nd International Conference on Sustainable Development in Civil, Urban and Transportation Engineering*, Ho Chi Minh City, Vietnam, vol. 143, pp. 1-12, 2018. [CrossRef] [Google Scholar] [Publisher Link]

[9] A. Farahmand, and A. AghaKouchak, "A Satellite-Based Global Landslide Model," *Natural Hazards and Earth System Sciences*, vol. 13, no. 5, pp. 1259-1267, 2013. [CrossRef] [Google Scholar] [Publisher Link]

[10] Rafi Ullah et al., "Assessment of Residual Soil Properties for Slope Stability Analysis," *International Journal of Geomate*, vol. 21, no. 86, pp. 72-80, 2021. [Google Scholar] [Publisher Link]

[11] Tehseena Ali, Himanshu Rana, and G. L. Sivakumar Babu, "Analysis of Rainfall-Induced Shallow Slope Failure," *Proceedings of the Indian Geotechnical Conference 2019*, pp. 679-691, 2021. [CrossRef] [Google Scholar] [Publisher Link]

[12] Javier Bustamante et al., "Sensitivity Analysis of the Influence of Heavy-Intensity Rain Duration on the Stability of Granular Soil Slopes Under Unsaturated Conditions," *Applied Sciences*, vol. 15, no. 11, pp. 1-18, 2025. [CrossRef] [Google Scholar] [Publisher Link]

[13] Anabel Castro et al., "*Climates of Peru: Climate Classification Map*," Report, National Meteorology and Hydrology Service of Peru, pp. 1-70, 2021. [Google Scholar] [Publisher Link]

[14] Cesar Aybar et al., "Construction of a High-Resolution Gridded Rainfall Dataset for Peru from 1981 to the Present Day," *Hydrological Sciences Journal*, vol. 65, no. 5, pp. 770-785, 2020. [CrossRef] [Google Scholar] [Publisher Link]

[15] Rosario Belen Huarcaya Quiquia, and Emerson Raul Lucas Gonzales, "*Influence of Unsaturated Soil Parameters on the Infiltration and Stability Analysis of a Leaching Heap with a High Fines Content*," Thesis, Pontifical Catholic University of Peru, pp. 1-152, 2024. [Google Scholar] [Publisher Link]

[16] Josif Josifovski, and Stanislav Lenart, "Some Experience in Numerical Modelling of Unsaturated Slope Instabilities," *E3S Web Conference*, vol. 9, 2016. [CrossRef] [Google Scholar] [Publisher Link]

[17] Nichirvan Ramadhan Taher et al., "Numerical Investigation of the Effect of Slope Angle and Height on the Stability of a Slope Composed of Sandy Soil," *Proceedings of the 7th International Erciyes Conference on Scientific Research*, vol. 12, no. 2, pp. 664-675, 2022. [CrossRef] [Google Scholar] [Publisher Link]

[18] Ministry of Transport and Communications, "*Directorate General of Roads and Railways Highway Manual: Geometric Design*," pp. 1-285, 2018. [Google Scholar] [Publisher Link]

[19] Jinke Yuan et al., "Runoff and Soil Loss Characteristics on Sandy Soil Slope with New Chemical Sand-Fixing Agent under Simulated Rainfall," *Environmental Earth Sciences*, vol. 82, vol. 11, 2023. [CrossRef] [Google Scholar] [Publisher Link]

[20] Tzuri Eilat et al., "A Comparative Study of Embedded Wall Displacements Using Small-Strain Hardening Soil Model," *Geotechnics*, vol. 4, no. 1, pp. 309-321, 2024. [CrossRef] [Google Scholar] [Publisher Link]

[21] T. Schanz, P.A. Vermeer, and P.G. Bonnier, *The Hardening Soil Model: Formulation and Verification*, Beyond 2000 in Computational Geotechnics, Routledge, pp. 1-16, 2019. [CrossRef] [Google Scholar] [Publisher Link]

[22] M. Th. Van Genuchten, "A Closed-form Equation for Predicting the Hydraulic Conductivity of Unsaturated Soils," *Soil Science Society of America Journal*, vol. 44, no. 5, pp. 892-898, 1980. [CrossRef] [Google Scholar] [Publisher Link]

[23] Gerardo Bustos Pretel, *PG-3 General Technical Specifications for Road and Bridge Works*, Liteam, pp. 1-696, 2002. [Google Scholar] [Publisher Link]

[24] Esteban Litvin, "*Numerical Analysis of the Effect of Rainfall Infiltration on Slope Stability*," Geotechnical Engineer, Atkins, pp. 38-41, 2008. [Google Scholar] [Publisher Link]

[25] Zhuolin Wu et al., "Numerical Simulation Study of Rainfall-Induced Saturated–Unsaturated Landslide Instability and Failure," *Water*, vol. 17, no. 15, pp. 1-20, 2025. [CrossRef] [Google Scholar] [Publisher Link]

[26] E. Imre et al., *Using Grain Size Distribution to Estimate Permeability*, Geotechnical Engineering Challenges to Meet Current and Emerging Needs of Society, 1st ed., CRC Press, pp. 1-4, 2024. [CrossRef] [Google Scholar] [Publisher Link]

[27] Jesús Díaz-Curiel et al., "New Granulometric Expressions for Estimating Permeability of Granular Drainages," *Bulletin of Engineering Geology and the Environment*, vol. 81, no. 10, pp. 1-15, 2022. [CrossRef] [Google Scholar] [Publisher Link]

[28] Joram Wachira Mburu et al., "Investigations of Unsaturated Slopes Subjected to Rainfall Infiltration Using Numerical Approaches-A Parametric Study and Comparative Review," *Sustainability*, vol. 14, no. 21, pp. 1-37, 2022. [CrossRef] [Google Scholar] [Publisher Link]

[29] Gaoliang Tao et al., "Assessment of Vegetation Cover and Rainfall Infiltration Effects on Slope Stability," *Applied Sciences*, vol. 15, no. 17, pp. 1-25, 2025. [CrossRef] [Google Scholar] [Publisher Link]